

Article

Gas Hydrate Occurrence Inferred from Dissolved Cl^- Concentrations and $\delta^{18}\text{O}$ Values of Pore Water and Dissolved Sulfate in the Shallow Sediments of the Pockmark Field in Southwestern Xisha Uplift, Northern South China Sea

Min Luo^{1,2}, Linying Chen³, Hongpeng Tong³, Wen Yan³ and Duofu Chen^{1,3,*}

¹ Key Laboratory of Marginal Sea Geology, Guangzhou Institute of Geochemistry, Chinese Academy of Sciences, Guangzhou 510640, China; E-Mail: luomin@gig.ac.cn

² University of Chinese Academy of Sciences, Beijing 100049, China

³ Key Laboratory of Marginal Sea Geology, South China Sea Institute of Oceanology, Chinese Academy of Sciences, Guangzhou 510301, China; E-Mails: cly2812@hotmail.com (L.C.); tonghp@scsio.ac.cn (H.T.); wyan@scsio.ac.cn (W.Y.)

* Author to whom correspondence should be addressed; E-Mail: cdf@gig.ac.cn; Tel.: +86-20-8529-0286; Fax: +86-20-8529-0130.

Received: 19 February 2014; in revised form: 26 May 2014 / Accepted: 3 June 2014 / Published: 20 June 2014

Abstract: Deep-water pockmarks are frequently accompanied by the occurrence of massive gas hydrates in shallow sediments. A decline in pore-water Cl^- concentration and rise in $\delta^{18}\text{O}$ value provide compelling evidence for the gas hydrate dissociation. Mega-pockmarks are widely scattered in the southwestern Xisha Uplift, northern South China Sea (SCS). Pore water collected from a gravity-core inside of a mega-pockmark exhibits a downward Cl^- concentration decrease concomitant with an increase in $\delta^{18}\text{O}$ value at the interval of 5.7–6.7 mbsf. Concentrations of Cl^- , Na^+ , and K^+ mainly cluster along the seawater freshening line without distinct Na^+ enrichment and K^+ depletion. Thus, we infer that the pore water anomalies of Cl^- concentrations and $\delta^{18}\text{O}$ values are attributed to gas hydrate dissociation instead of clay mineral dehydration. Moreover, the lower $\delta^{18}\text{O}$ values of sulfate in the target core (C14) than those in the reference core (C9) may be associated with the equilibrium oxygen fractionation during sulfate reduction between sulfate and the relatively ^{18}O -depleted ambient water resulting from gas hydrate formation. The gas hydrate contents are estimated to be 6%–10% and 7%–15%, respectively, according to the offset of Cl^- concentrations and $\delta^{18}\text{O}$ values from the baselines. This pockmark field in southwestern Xisha Uplift is likely to be a good prospective area for the occurrence of gas hydrate in shallow sediments.

Keywords: gas hydrate; pore water; chloride; $\delta^{18}\text{O}$; southwestern Xisha Uplift

1. Introduction

Pockmarks form when seabed fluid (generally methane-enriched) discharges through the seafloor by suspending and winnowing the fine-grained sediments. Methane-enriched fluid is likely to crystallize as gas hydrate when it is transported into the gas hydrate stability zone [1]. One-meter high submarine hydrate pingoes caused by the volume expansion when massive gas hydrate precipitated in shallow sediments of a pockmark were discovered via ROV visual documentation at Nyegga, in the Norwegian Sea [2]. In the Northern Congo Fan, southwestern Africa, the high reflection amplitudes in the sediment echosounder records suggested the presence of 25–30 m thick gas hydrate-bearing sediment section in a giant pockmark, which was demonstrated by gravity sediment coring [3]. Therefore, deep-water pockmarks are propitious locales for the generation of massive gas hydrates and could possibly play a significant role in guiding gas hydrate exploration.

Pore water geochemical anomalies are effective indicators for the presence of gas hydrates and have been widely utilized in gas hydrate exploration [4,5]. When gas hydrates crystallize in the sediment pore space from water and either the biogenic methane bacterially generated in the methanogenic zone or the thermogenic methane advected from greater depth, dissolved ions are excluded from the cage-like structure as water molecules are incorporated into gas hydrate, increasing the salinity, and more specifically the chlorinity of the pore waters. Meanwhile, solid-fluid isotope fractionation causes the preferential uptake of the heavy isotope ^{18}O in gas hydrates and depletion in the fluid [6]. Conversely, fresh water and ^{18}O -enriched fluid is released and mixes with surrounding pore water when gas hydrates dissociate due to the shift of temperature and pressure or sediment coring [7,8]. As a result, excursions to low chlorinity in the pore waters, concomitant with the positive anomalies in the oxygen isotopic composition of the water provide compelling evidence for gas hydrate dissociation. Additionally, these coupled anomalies are likely to give reliable quantitative estimates of gas hydrate concentration in the sediments [9,10].

Due to the high concentration of sulfate in the ocean, dissimilatory bacterial sulfate reduction (BSR) is responsible for the majority of organic matter oxidation, even if its free energy yield is much lower than those of aerobic oxidation, denitrification, and manganese and iron reduction [11,12]. In addition, a large amount of methane in the sediments is anaerobically oxidized by sulfate (AOM) mediated by a syntrophic consortium of methanotrophic archaea and sulfate-reducing bacteria [13,14]. BSR is a complex biogeochemical process which consists of at least four major intracellular reversibly steps [15]. One of the consequences of BSR is the enrichment of both ^{34}S and ^{18}O in the residual sulfate because bacteria discriminate against ^{34}S and ^{18}O isotopes to various degrees [16]. Knowledge of sulfur and oxygen isotopes of sulfate could not only provide insight into the mechanism of isotope fractionation during BSR, but also give clue to the change of ambient environment where BSR occurs.

A myriad of lines of geophysical and geochemical evidence for gas hydrate occurrence have been discovered in northern continental margin of the SCS during the comprehensive survey and research of the past 15 years [17,18]. Bottom simulating reflectors (BSRs) indicative of the phase boundary between free gas below and solid gas hydrate above are widely distributed in the Qiongdongnan Basin,

Pearl River Mouth Basin, and Southwestern Taiwan Basin [19–21]. Moreover, pore-water concentration anomalies of CH_4 , Ca^{2+} , Mg^{2+} , and Sr^{2+} , shallow depth of sulfate-methane interface, and authigenic carbonates occurrence in shallow sediments and on the seafloor suggest the possible existence of gas hydrates in the subsurface sediments [22–29]. However, indication for the presence of gas hydrates in shallow sediments has not yet been reported in the northern SCS.

Seabed pockmarks are widespread in the southwestern Xisha Uplift with a density of ca. $0.4\text{--}1\text{ km}^{-2}$. Some of them are so enormous that they are rare worldwide. The majority of these pockmarks measure 1000–2500 m in diameter and 60–140 m in depth. Their distribution is closely linked to underlying fluid migration structures, such as gas chimneys, faults, unconformities, depositional boundaries, polygonal faults, paleo-channels, *etc.* [30]. The study area is characterized by high sedimentation rates (up to 1.2 mm/yr) and high geothermal gradients ($39\text{--}41\text{ }^\circ\text{C}/\text{km}$) [31]. Due to rapid sediment loading and the resulting undercompaction, overpressure has built up throughout much of the study area. Additionally, high geothermal gradients have accelerated the maturity of source rock, thereby producing a great amount of hydrocarbon [32]. The seepage of overpressured fluid coupled with strong activity of bottom currents gave rise to the formation of mega-pockmarks in the study area [30]. The integrated analysis of concentration profiles of pore water species suggests that these mega-pockmarks may be presently inactive [33]. Nonetheless, it is still unclear that whether gas hydrates exist in the shallow sediments of this pockmark field or not.

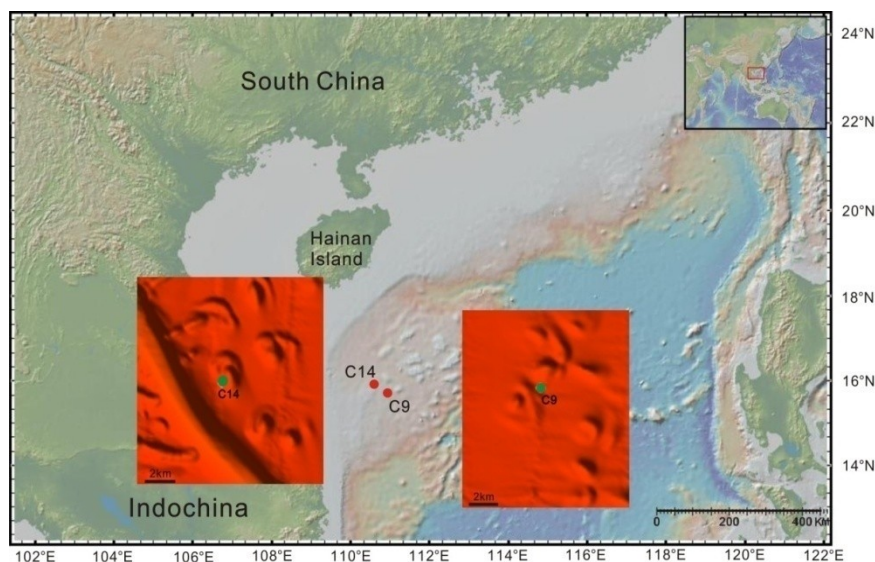
We detected the pore water anomalies of Cl^- concentrations and $\delta^{18}\text{O}$ values in a sediment core retrieved from the pockmark field in southwestern Xisha Uplift, northern SCS for the first time. The cause of these anomalies was then discussed to be linked to gas hydrate dissociation instead of to clay mineral dehydration via investigating the Na^+ and K^+ concentration profiles. $\delta^{18}\text{O}$ values of sulfate were provided as additional evidence supporting gas hydrate occurrence. Finally, we estimated the gas hydration concentrations through the anomalies of pore water Cl^- concentrations and $\delta^{18}\text{O}$ values.

2. Sampling and Methods

Two sediment cores were retrieved via gravity-piston corer from the southwestern Xisha Uplift, northern SCS during the Shiyun-1 Cruise by South China Sea Institute of Oceanology in May, 2012. C9 (7.6 m in length) as the reference core was obtained from outside a pockmark ($15^\circ41.032'\text{ N}$, $110^\circ57.246'\text{ E}$) with the water depth of 829 m. C14 (6.7 m in length) as the target core was collected at the flank of a giant pockmark ($15^\circ54.507'\text{ N}$, $110^\circ38.607'\text{ E}$) with the water depth of ~ 840 m (Figure 1). The homogeneous sediments are characterized by grayish-green foraminiferous silty clay.

After the corers were brought to the deck, core barrels were immediately removed and both ends of the PVC liners were capped. Pore water collection was done in the onboard laboratory by means of Rhizon samplers consisting of a hydrophilic, porous polymer tube. The tube was introduced into the sediments by its capillary-bearing part and the opposite end was connected to a ~ 20 mL syringe. Aliquots of pore water were preserved with 10 μL saturated HgCl_2 solution in two 10 mL glass vials. After N_2 was used to blow away the air in the headspace, all the aliquots of pore water were stored at $4\text{ }^\circ\text{C}$ in a refrigerator onboard.

Figure 1. Sampling location of sediment cores. The insets are the multibeam bathymetry maps showing sampling sites relative to pockmarks.



Concentrations of Cl^- , Na^+ , and K^+ as well as $\delta^{18}\text{O}$ values of pore water were measured at the State Key Laboratory of Isotope Geochemistry, Guangzhou Institute of Geochemistry, Chinese Academy of Sciences. Pore water samples were properly diluted (1:500 for Cl^- and 1:200 for Na^+ and K^+) with ultrapure water for determination of the concentrations of Cl^- , Na^+ , and K^+ using a Dionex ICS-900 ion chromatograph. The analytical precision is better than 2%. Pore water $\delta^{18}\text{O}$ values were determined adopting $\text{H}_2\text{O}-\text{CO}_2$ equilibration method using GV IsoPrime II isotope ratio mass spectrometer. The $\delta^{18}\text{O}$ values of pore water were calculated in per mil (‰) delta notation relative to V-SMOW. The analytical precision is $\pm 0.1\%$.

For the measurement of $\delta^{18}\text{O}$ values of sulfate, dissolved sulfate was precipitated as barium sulfate by the addition of an excess of barium chloride. The precipitate was carefully washed with ultra-pure water and freeze dried. The $\delta^{18}\text{O}$ values of barium sulfate were measured at Louisiana State University (Baton Rouge, LA, USA) via CO generated by a Thermal Conversion Elemental Analyzer at 1450 °C coupled with the MAT 253 in a continuous-flow mode. The $\delta^{18}\text{O}$ values are reported relative to V-SMOW and the precision for $\delta^{18}\text{O}$ is $\pm 0.5\%$.

3. Results

The measured concentrations of Cl^- , Na^+ , and K^+ , and $\delta^{18}\text{O}$ values of pore water and sulfate are listed in Table 1. Cl^- concentrations of C9 display little variation with depth ranging between 524 and 508 mM (Figure 2A). Na^+ and K^+ concentrations as well as pore water $\delta^{18}\text{O}$ values also change little in the whole core (Figure 2B–D). Cl^- concentrations of C14 are nearly constant till 5.7 mbsf (508 ± 8 mM), but they drop sharply below 5.7 mbsf (469 ± 8 mM) with a minimum of 453 mM (Figure 2A). Na^+ concentrations do not show great variation above 5.7 mbsf (437 ± 7 mM) and decrease slightly to 412 mM below 5.7 mbsf (Figure 2B). K^+ concentrations generally exhibit a gentle decline (9.5–8.7 mM) above 5.7 mbsf, and keep decreasing to 8.2 mM below 5.7 mbsf (Figure 2C). Pore water $\delta^{18}\text{O}$ values show a slight increase from 0.03‰ to 0.16‰ above 5.7 mbsf and continue increasing rapidly to the maximum

of 0.57‰ below 5.7 mbsf (Figure 2D). $\delta^{18}\text{O}$ values of sulfate monotonously increase from 10.7‰ to 21.6‰ for C9 and from 10.9‰ to 19.9‰ for C14 (Figure 3A).

Table 1. Variations of the concentrations of Cl^- , Na^+ , and K^+ as well as $\delta^{18}\text{O}$ values of pore water and sulfate in C9 and C14.

Depth(mbsf)	Cl^- (mM)	Na^+ (mM)	K^+ (mM)	$\delta^{18}\text{O}_{\text{H}_2\text{O}}$ (‰ V-SMOW)	$\delta^{18}\text{O}_{\text{SO}_4}$ (‰ V-SMOW)
C9					
0.06	519.9	465.9	9.9	0.05	10.7
0.42	517.2	463.5	9.7		
0.78	507.9	461.0	9.6		13.3
1.14	516.7	464.5	9.6		
1.50	523.7	468.6	9.8	0.03	
1.86	524.7	461.4	9.7		
2.22	514.7	459.7	9.6		18.4
2.58	516.4	468.4	9.3	0.1	
2.94	513.8	459.1	9.5		
3.30	517.6	457.1	9.3		
3.66	519.1	466.6	9.5	0.07	
4.02	520.1	460.7	9.6		20.3
4.38	522.8	458.8	9.8		
4.74	518.6	459.9	9.4	0.04	
5.10	516.9	451.9	9.5		
5.46	519.1	457.1	9.5		
5.82	523.3	468.6	9.5	0.06	20.6
6.18	516.6	461.3	9.7		
6.54	523.3	463.6	9.7		
6.90	508.5	459.6	9.8	0.07	21.6
7.26	518.5	455.7	9.6		
7.56	516.1	456.3	9.8	0.05	21.4
C14					
0.06	536.6	460.7	9.5		
0.18	529.3	445.4	9.3	0.03	10.9
0.3	512.5	441.9	9.2		
0.54	505.5	446.8	8.9		16.6
0.78	519	450.6	9.5		
1.02	513.1	443	8.8		17.3
1.2	504.5	433.3	8.9	0.03	
1.26	509.7	440.6	8.7		
1.5	499.4	443.8	9.2		
1.74	515.9	443.6	9.2		17.6
1.98	508.6	439.7	8.9		
2.22	508	443.4	9.1		
2.4	500	425.1	8.8	0.09	
2.82	508.4	432.8	8.8		18.5
3.3	504.3	429.6	8.7		

Table 1. Cont.

Depth(mbsf)	Cl ⁻ (mM)	Na ⁺ (mM)	K ⁺ (mM)	δ ¹⁸ O _{H2O} (‰ V-SMOW)	δ ¹⁸ O _{SO4} (‰ V-SMOW)
C14					
3.66	507.8	429.1	8.8	0.1	
3.78	513.9	435.6	9		
4.02	507.5	437.6	9.1		
4.26	502	435.8	9		19.4
4.5	504.5	431.5	8.8		
4.62	504.8	430.6	8.8		
4.8	501.8	425.4	9	0.16	
4.86	504.8	426.5	8.7		
5.1	503.6	429.4	8.9		
5.34	502.9	428	8.7		19.6
5.7	509.5	433.5	9	0.37	
5.88	478.7	431.5	8.9		
6.06	465.2	418.4	8.4	0.55	
6.3	458.6	415.9	8.3	0.51	
6.54	469.3	417.4	8.4		19.9
6.66	462.5	412.4	8.3	0.57	

Figure 2. Pore-water concentration profiles of Cl⁻ (A), Na⁺ (B), and K⁺ (C) as well as δ¹⁸O values (D) for C9 (blue) and C14 (red). The dash line in (D) representing the background trend of δ¹⁸O values is determined via polynomial fitting using measured pore water δ¹⁸O values above 5.7 mbsf.

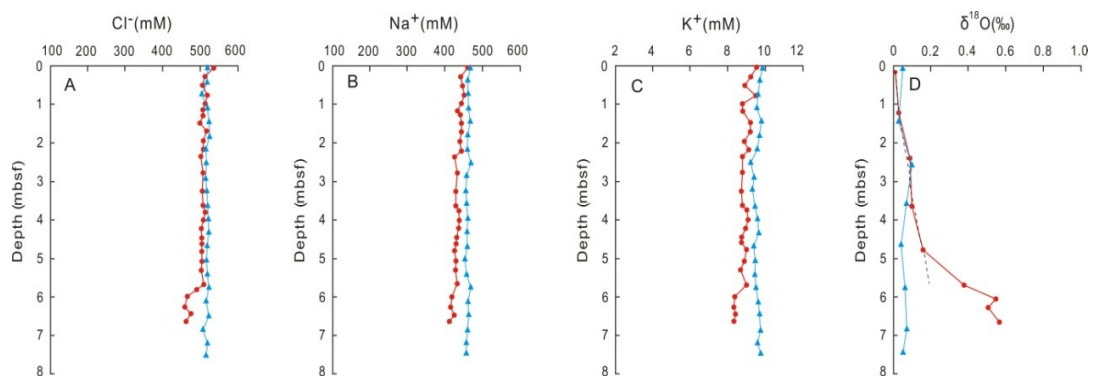
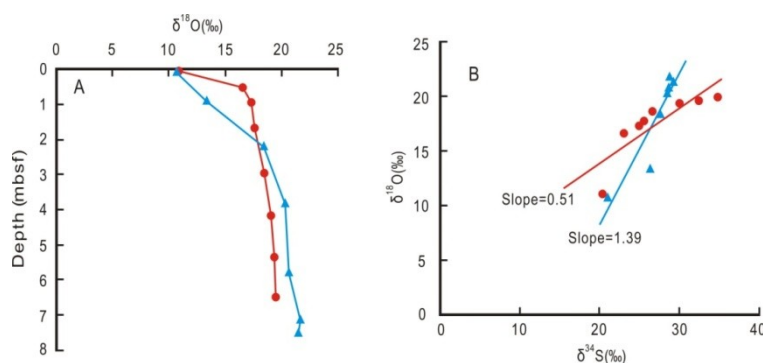


Figure 3. (A) δ¹⁸O values of sulfate in C9 (blue) and C14 (red); (B) δ¹⁸O_{SO4} vs. δ³⁴S_{SO4} data in pore water sulfate of C9 (blue) and C14 (red). δ³⁴S_{SO4} values were taken from Luo *et al.* [33].

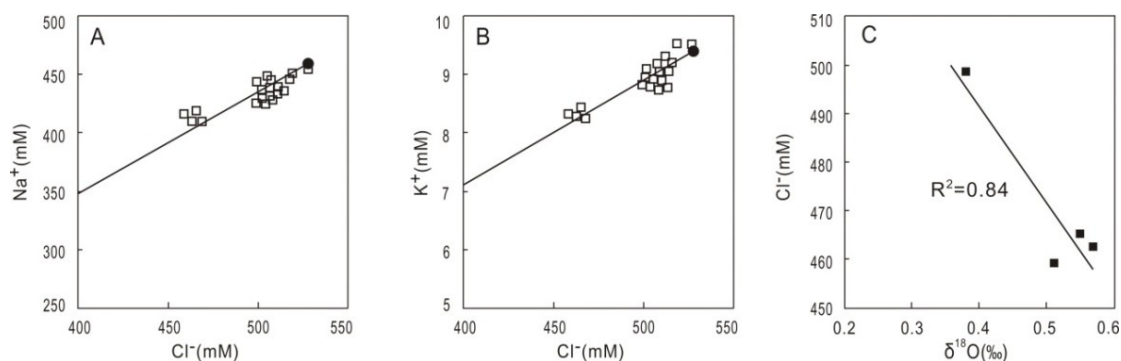


4. Discussion

4.1. Potential Occurrence of Gas Hydrates Inferred from Coupled Chlorinity Decrease and $\delta^{18}\text{O}$ Increase

Due to the salt exclusion effect and preferential uptake of heavy isotope ^{18}O in the solid phase when gas hydrates crystallize, fresh water would be released, thereby diluting the surrounding pore water as well as increasing the $\delta^{18}\text{O}$ values as gas hydrates decompose during core sample retrieval [6,8]. Therefore, coupled pore water chlorinity and $\delta^{18}\text{O}$ anomalies have been demonstrated to be typical signals of the presence of gas hydrate [7]. A myriad of studies have shown that pore water chlorinity and $\delta^{18}\text{O}$ anomalies are pervasive in gas hydrate occurrence areas worldwide, such as ODP Leg 112 Site 685 in the Peruvian continental margin [34], ODP Leg 164 Site 994 and 997 in Blake Ridge [9], the exploratory well in Nankai Trough [35], ODP Leg 204 Site 1245 and 1246 at Hydrate Ridge in the Cascadia margin [36], 41GC gravity sediment core in G11 pockmark offshore Mid-Norway [37]. Undoubtedly, pore water chlorinity decrease coupled with $\delta^{18}\text{O}$ increase is also typical for clay mineral dehydration, most likely for the transformation of smectite to illite [38,39]. However, Na^+ enrichment and K^+ depletion in surrounding pore water are believed to be a direct consequence of the transformation of clay mineral where Na^+ is released into solution but K^+ is integrated into illite [40–43]. Concentrations of Cl^- , Na^+ , and K^+ decrease in varying degree below 5.7 mbsf and the data primarily cluster along the seawater freshening line (Figure 4A,B). This observation is contradicted with the anomalies of pore water chlorinity and $\delta^{18}\text{O}$ caused by clay mineral dehydration, because the data in Figure 4A,B would generally scatter above or below the seawater freshening line due to Na^+ enrichment and K^+ depletion. Additionally, fluid migration channels, such as fractures, gas chimneys, polygonal faults, *etc.*, were widely recognized in the seismic profiles of the adjacent Qiongdongnan Basin and they created pathways for fluid flow both laterally and vertically to shallow sediments, providing the prerequisite for gas hydrates formation in shallow sediments [44–46]. Notably, dissolved Cl^- concentrations also show good correlation with $\delta^{18}\text{O}$ values (Figure 4C). Hence, we infer that the dissolved Cl^- concentrations decline along with $\delta^{18}\text{O}$ values rise could be caused by gas hydrate melting that discharged fresh water and ^{18}O -enriched fluid into interstitial water.

Figure 4. Plots of Cl^- vs. Na^+ (A), K^+ (B), and $\delta^{18}\text{O}$ (C). Solid circles in (A) and (B) indicate seawater values.



4.2. $\delta^{18}\text{O}$ Values of Sulfate as an Additional Indication for Possible Gas Hydrate Occurrence

Sulfur isotope fractionation during BSR is mainly governed by kinetic effects which are closely related to sulfate reduction rate [47], whereas oxygen isotope depends mainly on equilibrium fractionation which exchanges its isotope with ambient water although the possibility of kinetic fractionation cannot be fully precluded [48–50]. The relative evolution of the $\delta^{18}\text{O}_{\text{SO}_4}$ vs. $\delta^{34}\text{S}_{\text{SO}_4}$ has been suggested to be linked to the overall sulfate reduction rate [47,49]. At sites with high sulfate reduction rates, the $\delta^{18}\text{O}_{\text{SO}_4}$ increases more slowly relative to the $\delta^{34}\text{S}_{\text{SO}_4}$, while at sites with low sulfate reduction rates, the $\delta^{18}\text{O}_{\text{SO}_4}$ increases more quickly relative to the $\delta^{34}\text{S}_{\text{SO}_4}$. Therefore, higher sulfate reduction rate results in a lower slope on the plot of $\delta^{18}\text{O}_{\text{SO}_4}$ vs. $\delta^{34}\text{S}_{\text{SO}_4}$ in the residual sulfate pool [51,52]. The measured data of $\delta^{18}\text{O}$ and $\delta^{34}\text{S}$ of sulfate display a close-to-linear relationship both in C9 and C14 on the plot of $\delta^{18}\text{O}_{\text{SO}_4}$ vs. $\delta^{34}\text{S}_{\text{SO}_4}$ (Figure 3B). The slopes of both cores, however, are greatly different from each other (Figure 3B). The lower gradient probably suggests a higher sulfate reduction rate in C14 than in C9, which may be attributed to AOM occurrence in shallower sediment depth in C14. This observation confirms the deduce of Luo *et al.* [33] that AOM occurred in shallow sediments of C14 based on sulfate and DIC concentrations and $\delta^{34}\text{S}_{\text{SO}_4}$ values in both cores. AOM occurrence in shallow sediments implies a source of either biogenic methane generated by methanogenesis or thermogenic methane produced by thermal degradation of organic matter which is one of the prerequisites for gas hydrate formation. In addition, it is notable that the $\delta^{18}\text{O}_{\text{SO}_4}$ values in lower part of C9 are higher than those in C14 (Figure 3A). Previous studies have suggested that it is sulfite, one of the intercellular intermediates during sulfate reduction, that equilibratively exchanges oxygen isotope with ambient water and that some amount of sulfite is reoxidized to sulfate and releases back to the extracellular sulfate [49,50,53,54]. Therefore, we attribute the change in $\delta^{18}\text{O}_{\text{SO}_4}$ to the change in the $\delta^{18}\text{O}$ of ambient water. It is likely that the lower $\delta^{18}\text{O}_{\text{SO}_4}$ values were influenced by the relatively ^{18}O -depleted pore water during BSR after gas hydrate formation because ^{18}O in pore water is preferentially incorporated into gas hydrate lattice. However, oxygen isotope exchange reactions between sulfate and water were demonstrated to be extremely slow (10^7 years [55]) under typical marine environment without the enzymatically-activated microbial metabolism [48,56]. Heavy oxygen isotope released when gas hydrate dissociated thus may not be imprinted on oxygen isotopic compositions of sulfate because microbial activity was completely suppressed by adding HgCl_2 into the glass vials for pore water storage.

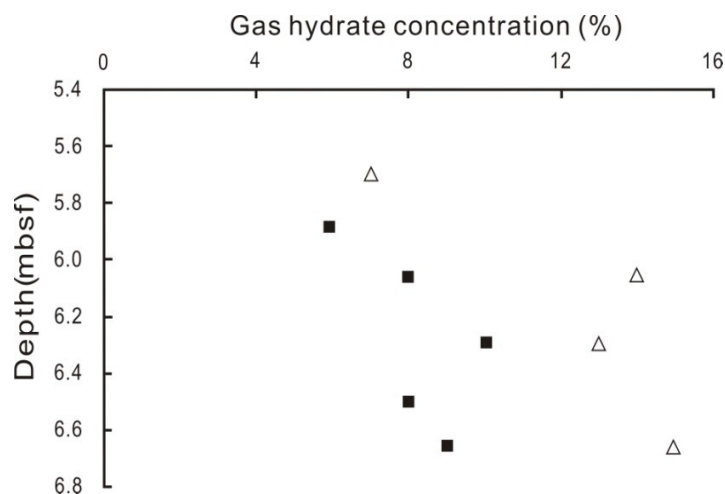
4.3. Gas Hydrate Contents Estimated from the Anomalies of Pore Water Chlorinity and $\delta^{18}\text{O}$ Values

As mentioned above, the pore water chlorinity decrease concomitant with $\delta^{18}\text{O}$ values increase are postulated to be caused by gas hydrate decomposition, so that the extent of decrease in chloride concentrations and increase in $\delta^{18}\text{O}$ values are proportional to the amount of gas hydrates that have dissociated [10,57]. Considering that there is no significant variation of Cl^- concentrations above 5.7 mbsf, we take the average of all the Cl^- concentrations above 5.7 mbsf (508 mM) as the Cl^- background concentration before hydrate dissociation. The gas hydrate content of the sediments (percentage by pore space) was calculated by the formula:

$$M = \left(1 - \frac{[\text{Cl}^-]_m}{[\text{Cl}^-]_b}\right) \times 100 \quad (1)$$

where M represents the gas hydrate concentration relative to pore space; $[Cl^-]_m$ represents the measured Cl^- concentration of pore water; and $[Cl^-]_b$ represents the baseline Cl^- concentration. According to Equation (1) and Cl^- concentrations below 5.7 mbsf, the estimated gas hydrate contents are within 6% and 10% with the average of 8% (Figure 5).

Figure 5. The estimated gas hydrate concentrations below 5.7 mbsf. Solid squares and open triangles represent the results derived from Cl^- concentrations and $\delta^{18}O$ values, respectively.



The pore water $\delta^{18}O$ anomalies as pointed out above are interpreted as the results of mixing of in-situ pore water unaffected by gas hydrate with heavy $\delta^{18}O$ water released by the dissociation of gas hydrate. Assuming that the gas hydrate has a stoichiometric composition as $CH_4 \cdot 5.75H_2O$ and the density of methane hydrate is 0.91 g/cm^3 [58], the volume ratio of gas hydrate water to gas hydrate is 0.79 accordingly. Based on the measured pore water $\delta^{18}O$ values, the estimated gas hydrate concentration is described as:

$$(1 - 0.21M) \times \delta^{18}O_m = 0.79M \times \delta^{18}O_h + (1 - M) \times \delta^{18}O_b \quad (2)$$

where M is the fraction of pore space occupied by gas hydrate; $\delta^{18}O_m$ is the measured pore water $\delta^{18}O$ value; $\delta^{18}O_h$ is the $\delta^{18}O$ value of gas hydrate-bound water; $\delta^{18}O_b$ is the background $\delta^{18}O$ value of pore water prior to gas hydrate decomposition. Although the $\delta^{18}O$ of modern seawater is ~ 0 , the background $\delta^{18}O$ value of pore water may deviate slightly from this value owing to the influence of seawater $\delta^{18}O$ value in geologic past. Thus, the $\delta^{18}O_b$ (0.19‰) is based on best-fit polynomial function using measured pore water $\delta^{18}O$ values above 5.7 mbsf (Figure 2D). According to the oxygen isotope fractionation equation between gas hydrate and pore water:

$$\delta^{18}O_h - \delta^{18}O_b = 1000 \ln \alpha = 1000(\alpha - 1) \quad (3)$$

$$\text{we get } \delta^{18}O_h = 1000(\alpha - 1) + \delta^{18}O_b \quad (4)$$

where α is the fractionation factor between gas hydrate and pore water and it was determined to be 1.003 [59]. Combining Equations (2) and (4) gives:

$$M = \frac{\delta^{18}O_m - \delta^{18}O_b}{[790(\alpha - 1) + 0.21(\delta^{18}O_m - \delta^{18}O_b)]} \quad (5)$$

The gas hydrate amounts (pore space %) were calculated to be 7%–15% with an average of 12% (Figure 5). The gas hydrate contents estimated using increased pore water $\delta^{18}\text{O}$ values are somewhat higher than those estimated through decreased Cl^- concentrations, which may result from salt ions trapped between rapidly grown hydrate crystals or incomplete salt exclusion [60,61]. Even if the gas hydrate contents are relatively high based both on reduced Cl^- concentrations and on increased $\delta^{18}\text{O}$ values, gas hydrates were not observed in C14 sediment core onboard. This is possibly attributed to the limited pore space in the hemipelagic-pelagic sediments so that finely disseminated hydrates rather than massive hydrates prevail in C14 below 5.7 mbsf.

5. Conclusions

Through the measurement of pore water concentrations of Cl^- , Na^+ , and K^+ as well as $\delta^{18}\text{O}$ values of pore water and dissolved sulfate obtained from shallow sediments of pockmark field in the southwestern Xisha Uplift, SCS, we discover compelling indicators for gas hydrate dissociation- Cl^- concentration decrease coupled with $\delta^{18}\text{O}$ values increase. Moreover, we precluded the possibility that the anomalies of pore water Cl^- concentrations and $\delta^{18}\text{O}$ values are due to clay mineral dehydration by incorporating investigation of Na^+ and K^+ concentration profiles. The difference between $\delta^{18}\text{O}$ values of sulfate in the reference core (C9) and the target core (C14) may be an additional indication for gas hydrate occurrence. Gas hydrates occupy 6%–10% and 7%–15% of pore-space volume within sediments, respectively, based on the deviation of Cl^- concentrations and $\delta^{18}\text{O}$ values from the baselines. Consequently, the pockmark field in the southwestern Xisha Uplift, northern SCS, is a potential area exhibiting favorable prospects for gas hydrate exploration.

Acknowledgments

We are grateful to Luhua Xie, Wenfeng Deng, and Qingxian Wang for their help in the measurement of pore water species. This study was funded by NSFC (Grants: 91228206 and 41306044) and GIGCAS 135 Project (Y234021001).

Author Contributions

All coauthors have been involved with the work, approved the manuscript, and agreed to its submission. Duofu Chen will be the corresponding authors. The paper is original and has not been and will not be submitted elsewhere.

Conflicts of Interest

The authors declare no conflict of interest.

References

1. Judd, A.G.; Hovland, M. *Seabed Fluid Flow: The Impact of Geology, Biology and the Marine Environment*; Cambridge University Press: Cambridge, UK, 2007.
2. Hovland, M.; Svensen, H. Submarine pingoes: Indicators of shallow gas hydrates in a pockmark at Nyegga, Norwegian Sea. *Mar. Geol.* **2006**, *228*, 15–23.

3. Sahling, H.; Bohrmann, G.; Spiess, V.; Bialas, J.; Breitzke, M.; Ivanov, M.; Kasten, S.; Krastel, S.; Schneider, R. Pockmarks in the Northern Congo Fan area, SW Africa: Complex seafloor features shaped by fluid flow. *Mar. Geol.* **2008**, *249*, 206–225.
4. Kastner, M.; Claypool, G.; Robertson, G. Geochemical constraints on the origin of the pore fluids and gas hydrate distribution at Atwater Valley and Keathley Canyon, northern Gulf of Mexico. *Mar. Pet. Geol.* **2008**, *25*, 860–872.
5. Borowski, W.S.; Paull, C.K.; Ussler, W. Carbon cycling within the upper methanogenic zone of continental rise sediments; an example from the methane-rich sediments overlying the Blake Ridge gas hydrate deposits. *Mar. Chem.* **1997**, *57*, 299–311.
6. Hesse, R.; Harrison, W.E. Gas hydrates (clathrates) causing pore-water freshening and oxygen-isotope fractionation in deepwater sedimentary sections of terrigenous continental margins. *Earth Planet. Sci. Lett.* **1981**, *55*, 453–462.
7. Hesse, R. Pore water anomalies of submarine gas-hydrate zones as tool to assess hydrate abundance and distribution in the subsurface—What have we learned in the past decade? *Earth-Sci. Rev.* **2003**, *61*, 149–179.
8. Ussler, W.; Paull, C.K. Effects of ion-exclusion and isotopic fractionation on pore-water geochemistry during gas hydrate formation and decomposition. *Geo-Mar. Lett.* **1995**, *15*, 37–44.
9. Matsumoto, R.; Borowski, W. Gas hydrate estimates from newly determined oxygen isotopic fractionation ($\alpha_{\text{GH-IW}}$) and $\delta^{18}\text{O}$ anomalies of the interstitial waters: Leg 164, Blake Ridge. *Proc. Ocean Drill. Program. Sci. Result.* **2000**, *164*, 59–66. Available online: http://www-odp.tamu.edu/publications/164_SR/VOLUME/CHAPTERS/SR164_06.PDF (accessed on 10 May 2013).
10. Kastner, M.; Kvenvolden, K.A.; Whiticar, M.J.; Camerlenghi, A.; Lorenson, T.D. Relation between pore fluids chemistry and gas hydrates associated with bottom simulating reflectors at the Cascadia margin, site 889 and 892. *Proc. Ocean Drill. Program. Sci. Result.* **1995**, *146*, 175–187. Available online: http://www-odp.tamu.edu/publications/146_1_SR/VOLUME/CHAPTERS/sr146pt1_10.pdf (accessed on 10 May 2013).
11. Froelich, P.N.; Klinkhammer, G.P.; Bender, M.L.; Luedtke, N.A.; Heath, G.R.; Cullen, D.; Dauphin, P. Early oxidation of organic matter in pelagic sediments of the eastern equatorial Atlantic: Suboxic diagenesis. *Geochim. Cosmochim. Acta* **1979**, *43*, 1075–1090.
12. Berner, R.A. *Early Diagenesis: A Theoretical Approach*; Princeton University Press: Princeton, NJ, USA, 1980.
13. Boetius, A.; Ravensschlag, K.; Schubert, C.J.; Rickert, D.; Widdel, F.; Gieseke, A.; Amann, R.; Jørgensen, B.B.; Witte, U.; Pfannkuche, O. A marine microbial consortium apparently mediating anaerobic oxidation of methane. *Nature* **2000**, *407*, 623–626.
14. Hoehler, T.M.; Alperin, M.J.; Albert, D.B.; Martens, C.S. Field and laboratory studies of methane oxidation in an anoxic marine sediment: Evidence for a methanogen-sulfate reducer consortium. *Glob. Biogeochem. Cycles* **1994**, *8*, 451–463.
15. Canfield, D. Biogeochemistry of sulfur isotopes. *Rev. Mineral. Geochem.* **2001**, *43*, 607–636.
16. Harrison, A.; Thode, H. Mechanism of the bacterial reduction of sulphate from isotope fractionation studies. *Trans. Faraday Soc.* **1958**, *54*, 84–92.
17. Luo, M.; Wang, H.; Yang, S.; Chen, D. Research advancement of natural gas hydrate in South China Sea. *Bull. Mineral. Petrol. Geochem.* **2013**, *32*, 56–69 (in Chinese with English abstract).

18. Wu, N.; Zhang, G.; Liang, J.; Su, Z.; Wu, D.; Lu, H.; Lu, J.; Sha, Z.; Fu, S.; Gong, Y.; *et al.* Progress of gas hydrate research in Northern South China Sea. *Adv. New Renew. Energy* **2013**, *1*, 80–94 (in Chinese with English abstract).
19. Xu, H.; Li, L.; Shu, H.; Wen, P.; Zhang, B. The seismic reflecting characteristics of gas hydrate bearing strata and its possible distribution in the South China Sea. *Appl. Geophys.* **2006**, *3*, 42–47.
20. Wu, S.; Zhang, G.; Huang, Y.; Liang, J.; Wong, H.K. Gas hydrate occurrence on the continental slope of the northern South China Sea. *Mar. Pet. Geol.* **2005**, *22*, 403–412.
21. Li, L.; Lei, X.; Zhang, X.; Zhang, G. Heat flow derived from BSR and its implications for gas hydrate stability zone in Shenhu Area of northern South China Sea. *Mar. Geophys. Res.* **2012**, *33*, 77–87.
22. Sun, C.; Wang, H.; Niu, B.; Huang, X. Geochemical prospecting of gas hydrate at Xisha Ocean Trough. *Earth Sci.-J. China Univ. Geosci.* **2004**, *29*, 135–140 (in Chinese with English abstract).
23. Fu, S. Gas origin constraint on the formation of gas hydrate. *Earth Sci. Front.* **2005**, *12*, 263–267 (in Chinese with English abstract).
24. Wu, N.; Zhang, H.; Yang, S.; Zhang, G.; Liang, J. Gas hydrate system of shenhu area, Northern South China Sea: Geochemical results. *J. Geophys. Res.* **2011**, *1*, 1–8.
25. Wu, L.; Yang, S.; Liang, J.; Su, X.; Fu, S.; Sha, Z.; Yang, T. Variations of pore water sulfate gradients in sediments as indicator for underlying gas hydrate in Shenhu Area, the South China Sea. *Sci. China* **2013**, *56*, 530–540.
26. Yang, T.; Jiang, S.; Ge, L.; Yang, J.; Ling, H.; Wu, N.; Zhang, G.; Liu, J.; Chen, D. Geochemical characteristics of sediment pore water from Site XS-01 in the Xisha Trough of South China Sea and the significance for gas hydrate occurrence. *Quat. Sci.* **2006**, *26*, 442–448 (in Chinese with English abstract).
27. Yang, T.; Jiang, S.; Ge, L.; Yang, J.; Wu, N.; Zhang, G.; Liu, J. Pore water geochemistry in the shallow sediments of Shenhu Area, northern South China Sea and its significance for the occurrence of gas Hydrates. *Chin. Sci. Bull.* **2009**, *54*, 3231–3240 (in Chinese with English abstract).
28. Han, X.; Suess, E.; Huang, Y.; Wu, N.; Bohrmann, G.; Su, X.; Eisenhauer, A.; Rehder, G.; Fang, Y. Jiulong methane reef: Microbial mediation of seep carbonates in the South China Sea. *Mar. Geol.* **2008**, *249*, 243–256.
29. Tong, H.; Feng, D.; Cheng, H.; Yang, S.; Wang, H.; Min, A.G.; Lawrence Edwards, R.; Chen, Z.; Chen, D. Authigenic carbonates from seeps on the northern continental slope of the South China Sea: New insights into fluid sources and geochronology. *Mar. Pet. Geol.* **2013**, *43*, 260–271.
30. Sun, Q.L.; Wu, S.G.; Hovland, M.; Luo, P.; Lu, Y.T.; Qu, T.L. The morphologies and genesis of mega-pockmarks near the Xisha Uplift, South China Sea. *Mar. Pet. Geol.* **2011**, *28*, 1146–1156.
31. Zhu, W.; Huang, B.; Mi, L.; Wilkins, R.W.T.; Fu, N.; Xiao, X. Geochemistry, origin, and deep-water exploration potential of natural gases in the Pearl River Mouth and Qiongdongnan basins, South China Sea. *AAPG Bull.* **2009**, *93*, 741–761.
32. Huang, B.J.; Xiao, X.M.; Li, X.X. Geochemistry and origins of natural gases in the Yinggehai and Qiongdongnan basins, offshore South China Sea. *Org. Geochem.* **2003**, *34*, 1009–1025.
33. Luo, M.; Chen, L.; Wang, S.; Yan, W.; Wang, H.; Chen, D. Pockmark activity inferred from pore water geochemistry in shallow sediments of the pockmark field in southwestern Xisha Uplift, northwestern South China Sea. *Mar. Pet. Geol.* **2013**, *48*, 247–259.

34. Kastner, M.; Elderfield, H.; Martin, J.B.; Suess, E.; Kvenvolden, K.A.; Garrison, R.E. Diagenesis and interstitial-water chemistry at the Peruvian continental margin—major constituents and strontium isotopes. *Proc. Ocean Drill. Program. Sci. Result.* **1990**, *112*, 413–440. Available online: http://www-odp.tamu.edu/publications/112_SR/VOLUME/CHAPTERS/sr112_25.pdf (accessed on 17 March 2013).
35. Tomaru, H.; Matsumoto, R.; Lu, H.; Uchida, T. Geochemical process of gas hydrate formation in the Nankai Trough based on chloride and isotopic anomalies in interstitial water. *Resour. Geol.* **2004**, *54*, 45–51.
36. Tomaru, A.; Matsumoto, R.; Torres, M.E.; Borowski, W.S. Geological and geochemical constraints on the isotopic composition of interstitial waters from the Hydrate Ridge region, Cascadia Continental margin. *Proc. Ocean Drill. Program. Sci. Result.* **2006**, *204*, 1–20. Available online: http://www-odp.tamu.edu/publications/204_SR/VOLUME/CHAPTERS/109.PDF (accessed on 10 May 2013).
37. Chen, Y.; Ussler, W., III; Haflidason, H.; Lepland, A.; Rise, L.; Hovland, M.; Hjelstuen, B.O. Sources of methane inferred from pore-water delta C-13 of dissolved inorganic carbon in Pockmark G11, offshore Mid-Norway. *Chem. Geol.* **2010**, *275*, 127–138.
38. Sheppard, S.; Gilg, H. Stable isotope geochemistry of clay minerals. *Clay Miner.* **1996**, *31*, 1–24.
39. Dählmann, A.; de Lange, G. Fluid–sediment interactions at Eastern Mediterranean mud volcanoes: A stable isotope study from ODP Leg 160. *Earth Planet. Sci. Lett.* **2003**, *212*, 377–391.
40. Aloisi, G.; Drews, M.; Wallmann, K.; Bohrmann, G. Fluid expulsion from the Dvurechenskii mud volcano (Black Sea): Part I. Fluid sources and relevance to Li, B, Sr, I and dissolved inorganic nitrogen cycles. *Earth Planet. Sci. Lett.* **2004**, *225*, 347–363.
41. Godon, A.; Jendzejewski, N.; Castrec-Rouelle, M.; Dia, A.; Pineau, F.; Boulègue, J.; Javoy, M. Origin and evolution of fluids from mud volcanoes in the Barbados accretionary complex. *Geochim. Cosmochim. Acta* **2004**, *68*, 2153–2165.
42. Martin, J.B.; Kastner, M.; Henry, P.; Le Pichon, X.; Lallement, S. Chemical and isotopic evidence for sources of fluids in a mud volcano field seaward of the Barbados accretionary wedge. *J. Geophys. Res.* **1996**, *101*, 20325–20345.
43. Hensen, C.; Nuzzo, M.; Hornibrook, E.; Pinheiro, L.M.; Bock, B.; Magalhães, V.H.; Brückmann, W. Sources of mud volcano fluids in the Gulf of Cadiz—indications for hydrothermal imprint. *Geochim. Cosmochim. Acta* **2007**, *71*, 1232–1248.
44. Wang, X.; Wu, S.; Wang, D.; Ma, Y.; Yao, G.; Gong, Y. The role of polygonal faults in fluid migration and gas hydrate reservoir forming in Southeast Hainan Basin. *Oil Geophys. Prospect.* **2010**, *45*, 122–128 (in Chinese with English abstract).
45. Wang, X.; Wu, S.; Dong, D.; Gong, Y.; Chai, C. Characteristics of gas chimney and its relationship to gas hydrate in Qiongdongnan Basin. *Mar. Geol. Quat. Geol.* **2008**, *28*, 103–108 (in Chinese with English abstract).
46. Wang, X.; Wu, S.; Yuan, S.; Wang, D.; Ma, Y.; Yao, G.; Gong, Y.; Zhang, G. Geophysical signatures associated with fluid flow and gas hydrate occurrence in a tectonically quiescent sequence, Qiongdongnan Basin, South China Sea. *Geofluids* **2010**, *10*, 351–368.
47. Aharon, P.; Fu, B. Microbial sulfate reduction rates and sulfur and oxygen isotope fractionations at oil and gas seeps in deepwater Gulf of Mexico. *Geochim. Cosmochim. Acta* **2000**, *64*, 233–246.

48. Fritz, P.; Basharmal, G.; Drimmie, R.; Ibsen, J.; Qureshi, R. Oxygen isotope exchange between sulphate and water during bacterial reduction of sulphate. *Chem. Geol.* **1989**, *79*, 99–105.
49. Brunner, B.; Bernasconi, S.M.; Kleikemper, J.; Schroth, M.H. A model for oxygen and sulfur isotope fractionation in sulfate during bacterial sulfate reduction processes. *Geochim. Cosmochim. Acta* **2005**, *69*, 4773–4785.
50. Mangalo, M.; Meckenstock, R.U.; Stichler, W.; Einsiedl, F. Stable isotope fractionation during bacterial sulfate reduction is controlled by reoxidation of intermediates. *Geochim. Cosmochim. Acta* **2007**, *71*, 4161–4171.
51. Antler, G.; Turchyn, A.V.; Rennie, V.; Herut, B.; Sivan, O. Coupled sulfur and oxygen isotope insight into bacterial sulfate reduction in the natural environment. *Geochim. Cosmochim. Acta* **2013**, *118*, 98–117.
52. Feng, D.; Roberts, H.H. Geochemical characteristics of the barite deposits at cold seeps from the northern Gulf of Mexico continental slope. *Earth Planet. Sci. Lett.* **2011**, *309*, 89–99.
53. Mangalo, M.; Einsiedl, F.; Meckenstock, R.U.; Stichler, W. Influence of the enzyme dissimilatory sulfite reductase on stable isotope fractionation during sulfate reduction. *Geochim. Cosmochim. Acta* **2008**, *72*, 1513–1520.
54. Wortmann, U.G.; Chernyavsky, B.; Bernasconi, S.M.; Brunner, B.; Böttcher, M.E.; Swart, P.K. Oxygen isotope biogeochemistry of pore water sulfate in the deep biosphere: Dominance of isotope exchange reactions with ambient water during microbial sulfate reduction (ODP Site 1130). *Geochim. Cosmochim. Acta* **2007**, *71*, 4221–4232.
55. Chiba, H.; Sakai, H. Oxygen isotope exchange rate between dissolved sulfate and water at hydrothermal temperatures. *Geochim. Cosmochim. Acta* **1985**, *49*, 993–1000.
56. Gamsjager, H.; Murmann, R.K. *Advances in Inorganic and Bioinorganic Mechanisms*; Sykes, A.G., Ed.; Academic London: London, UK, 1983; pp. 317–381.
57. Hesse, R.; Frape, S.K.; Egeberg, P.K.; Matsumoto, R. Stable isotopic studies (Cl, O, and H) of interstitial waters from site 997, Blake Ridge gas hydrate field, west Atlantic. *Proc. Ocean Drill. Program. Sci. Result.* **2000**, *164*, 129–137. Available online: http://www-odp.tamu.edu/publications/164_SR/VOLUME/CHAPTERS/SR164_12.PDF (accessed on 13 May 2013).
58. MacDonald, G.J. The future of methane as an energy resource. *Annu. Rev. Energy* **1990**, *15*, 53–83.
59. Davidson, D.; Leaist, D.; Hesse, R. Oxygen-18 enrichment in the water of a clathrate hydrate. *Geochim. Cosmochim. Acta* **1983**, *47*, 2293–2295.
60. Pavlova, G.; Pashkina, V. Distribution of halogens in interstitial waters of the Sea of Okhotsk as related to hydrate generation. *Oceanology* **1989**, *29*, 329–333.
61. Hesse, R. Pore-water anomalies in gas hydrate-bearing sediments of the deeper continental margins: Facts and problems. *J. Incl. Phenom. Macrocycl. Chem.* **1990**, *8*, 117–138.